Current Status of the High Intensity Pulsed Spallation Neutron Source at J-PARC[*)]

Hiroshi TAKADA

J-PARC Center, Japan Atomic Energy Agency, 2-4 Shirakata, Tokai-mura, Naka-gun, Ibaraki 319-1195, Japan

(Received 11 June 2017 / Accepted 19 January 2018)

At the Japan Proton Accelerator Research Complex, a pulsed spallation neutron source has been providing neutron beams with high intensities and narrow pulse widths since 2008 for various materials science experiments. The neuron-pulse characteristics measured during early low-power operations indicated that this source is capable of providing the world's highest peak neutron intensities and pulse resolution at the 1-MW operation level, which is the goal of the facility. To achieve this operational goal, efforts have been underway to solve a critical issue affecting the target operation, *i.e.* mitigation of cavitation damages at the front end of the mercury target vessel, by injecting gas micro-bubbles and using a fast flow of the mercury through a narrow channel. Another issue is that the target vessel needs to be redesigned to ensure its robustness against the cyclic thermal stress produced by the temperature swings when the proton-beam trips because the water shroud surrounding the mercury target vessel failed during 500-kW operation in 2015.

Keywords: spallation neutron source, mercury target, moderator, para-hydrogen, decoupler, cavitation damage, pressure wave, micro-bubble, narrow channel

DOI: 10.1585/pfr.13.2505013

1. Introduction

At the Japan Proton Accelerator Research Complex (J-PARC), a pulsed spallation neutron source [1] driven by a 3-GeV proton beam with a repetition rate of 25 Hz has been in operation since 2008. The goal of this facility is to promote various research fields related to materials science, using a suit of state-of-the-art neutron instruments, by supplying high-intensity and short-pulse neutron beams. The facility aims to achieve steady and stable source operations at a power of 1 MW for 5000 h per year.

Key components of this source include a neutron-production mercury target and three types of cryogenic liquid-hydrogen moderators (20 K, 1.5 MPa) surrounded by a reflector with inner beryllium and outer iron. The moderator system has the following features [2]: (1) It contains 100% para-hydrogen, which increases the peak intensity of the pulse and decreases the pulse tail. (2) It has a cylindrical shape of 14 cm in diameter and 12 cm long, which provides high-intensity neutron beams with wide neutron-extraction angles up to 50.8° (coupled-type moderator). (3) It is surrounded with the neutron absorber made from an Ag-In-Cd alloy, which makes the pulse width narrower and the pulse tails lower (de-coupled-type moderator). (4) It includes a Cd sheet inside the de-coupled-type moderator vessel, which provides a narrower pulse shape (poisoned-type moderator).

The mercury target vessel is made from 316L stainless steel, and cavitation damage is produced at the 3-mm-thick front end of the target vessel by the pressure waves generated in the mercury by the injections of pulsed proton beams. This severely affects the lifetime of the target vessel; this effect is much more pronounced than the radiation embrittlement caused by the atomic displacement. Mitigating cavitation damage is a critical issue that must be addressed to achieve the goal of target operations for 5000 h per year at 1 MW. At J-PARC, we have developed a method using gas micro-bubbles to mitigate the cavitation damage [3–6]. Notably, the displacement velocities induced in the target vessel by the pressure waves have been reduced by a factor of 3 - 4 [7, 8]. Moreover, the front-end of the target was changed from a single-wall to a double-wall structure that contains a narrow flow channel, which is 2 mm wide [9]. This type of target helps in suppressing the growth of cavitation bubbles by the faster mercury flow in the narrow channel. The modified target vessel was first used in the fall of 2014. The Spallation Neutron Source (SNS) [10] at Oak Ridge National Laboratory (ORNL) has already accomplished a user program at 1 MW using a similar mercury target with a narrow-channel structure [11].

Figure 1 shows the operational beam-power history of the neutron source at J-PARC. In January 2015, a 1-MW-equivalent proton-beam pulse was injected onto the mercury target for the first time. The beam power for the user program was increased to 500 kW in April 2015. However, the water shroud surrounding the mercury vessel failed

author's e-mail: takada.hiroshi90@jaea.go.jp

*) This article is based on the presentation at the Conference on Laser Energy Science / Laser and Accelerator Neutron Sources and Applications 2017.

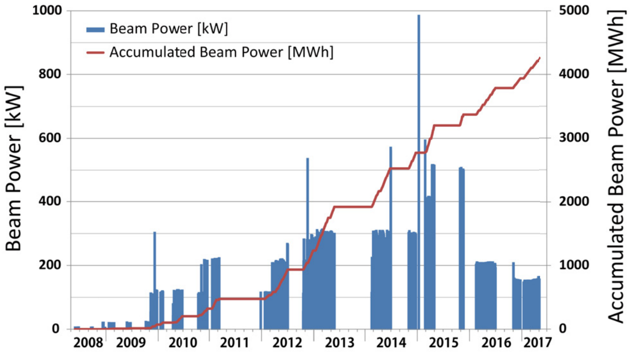

Fig. 1 Operational history of the neutron source at J-PARC as of March 31, 2017.

twice, interrupting the user program for about 4 months in total [12]. After these failures, the operational beam power was reduced to 200 kW because the spare target vessel having a more-reliable water shroud was not equipped with the gas-micro-bubble injection device needed for higher-power operation. Therefore, the target vessel needed to be urgently redesigned to produces a much more robust structure.

In this paper, we provide an overview of the distinctive neutronic characteristics of the moderators and the efforts to improve the robustness of the mercury target structure.

2. Outline of the Pulsed Neutron Source at J-PARC

Figure 2 shows a 3D view of the neutron-source station with an enlargement of the mercury target and the liquid-hydrogen moderators surrounded by the reflector. The mercury target is inserted into a helium vessel, forming a wing-type configuration with three moderators at the center. The side surface of the moderator is the origin of the neutron beamline. The front and back surfaces of the moderator are used as the viewed surface and the origin of the neutron beamline, respectively. At J-PARC, 23 neutron beamlines are arranged from six points of origin on the three moderators. Outside the helium vessel, a steel neutron-beam shutter, 2 m in length and 4 m in height, was installed on each neutron beamline. It moves vertically with a 1-m stroke to open and/or close the beamline. The helium vessel has a proton-beam insertion hole in front of the target, and the helium environment in the vessel is isolated from the proton-beam transport line by a proton-beam window made from aluminum alloy.

The target, moderators and reflector must be replaced by remotely-controlled tools before reaching their designed lifetimes. Horizontal access was selected for target-vessel replacement, whereas vertical access was chosen for the replacement of the moderator-reflector system, allowing us to replace the target vessel without the need of simultaneously handling the moderators and reflector.

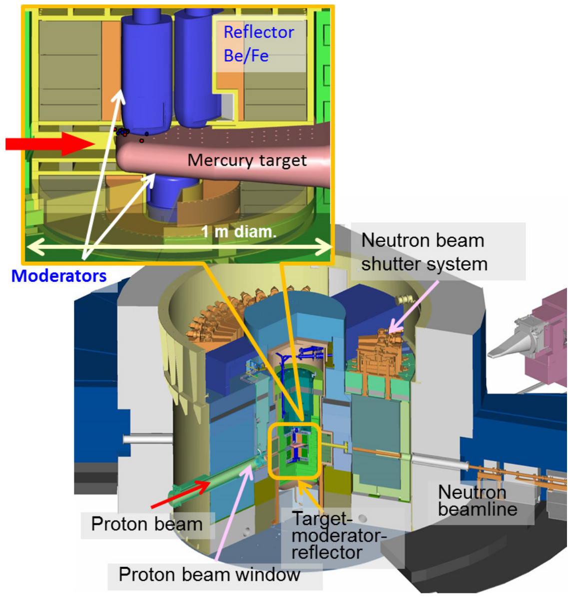

Fig. 2 3D view of the neutron-source station at J-PARC.

The shielding structure including the neutron beam shutters surrounding the target-moderator-reflector system was designed using 3D Monte-Carlo simulations, in which the geometry of all components was exactly modeled to meet the shielding-design criterion of keeping the dose rate less than 2.5 μSv/h at the biological shield surface [13].

3. Features of the Moderator-Reflector System

The moderator size was optimized to generate cold neutron beams with high intensities and good pulse-shapes using 100% para-hydrogen. Figure 3 shows the total neutron cross section in the energy range from eV to meV. The cross section is low for para-hydrogen, but incoming neutron losses about 15 meV *via* the conversion of para- to ortho-hydrogen when it interacts with para-hydrogen. This is an advantageous characteristic in view of slowing down the neutron. Instead, the moderator size becomes larger because the mean free path of neutrons with energies below tens of meV is longer in para-hydrogen due to its lower neutron cross sections.

Figure 4 shows the calculated neutron intensity relative to the neutron spectra for normal (75% ortho- and 25% para-) hydrogen and for different para-hydrogen concentrations. According to the energy dependence of the cross section, the neutron intensity increases in the energy region below 50 meV as the para-hydrogen fraction increases, with the 100% para-hydrogen case yielding the maximum. Note that the neutron intensity at approximately 10 meV is considerably enhanced. Figure 5 shows the calculated results for the neutron-pulse intensity emitted from the viewed surface of 10 cm × 10 cm of a moderator containing 100% para-hydrogen of different thick-

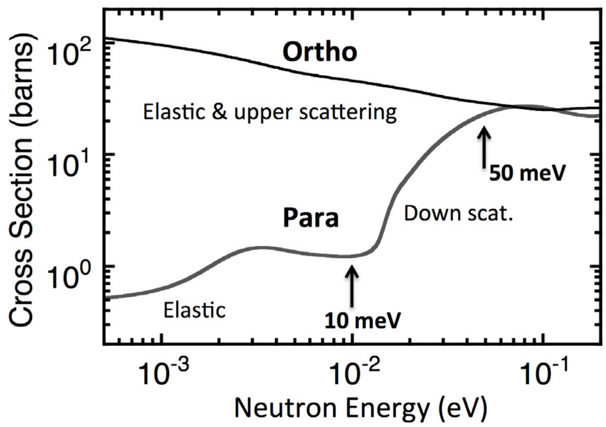

Fig. 3 Total neutron cross sections for para- and ortho-hydrogen [14].

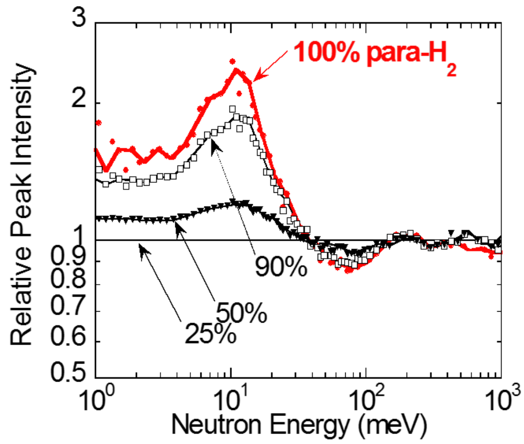

Fig. 4 Neutron intensity spectra calculated for different para-hydrogen concentration [15]. The result for the 25% para-hydrogen case is normalized to unity.

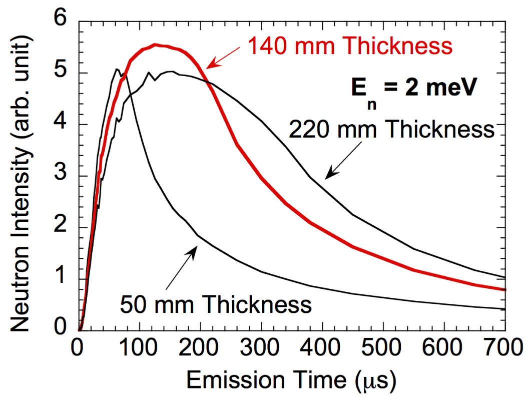

Fig. 5 Calculated neutron-pulse shape of a 2-meV neutron beam for different thickness of a 100% para-hydrogen moderator with a viewed surface of 10 cm × 10 cm [16].

nesses. The neutron intensity is maximum for the case with a 140-cm thickness.

Typically, rectangular-shaped moderators are used in the existing pulsed spallation neutron sources. However, a cylindrical moderator may provide a higher neutron intensity than the rectangular type at a large viewed angle [16]. As shown in Fig. 6, the neutron intensity at a viewed angle of 25° is almost equal to that at the central angle (0°) for the cylindrical geometry. For the rectangular geometry, in contrast, the neutron intensity decreases more rapidly at the viewed angle of 25°, as the distance from the axis perpendicular to the center of the moderator surface increases. Based on this result, a cylindrical shape was adopted for the first time for the moderator at J-PARC. Ultimately, for the coupled moderator, six neutron instruments were arranged in a wide angular range up to 50.8° from one side, and five neutron instruments in the range up to 45° from the other, by optimizing neutron-beam shutter design. The neutron-pulse characteristics from the coupled moderator were measured during low-power operation, and they indicated that a neutron intensity as high as 4.5×10^{12} n/cm^2/s/sr can be obtained during 1-MW operation [17].

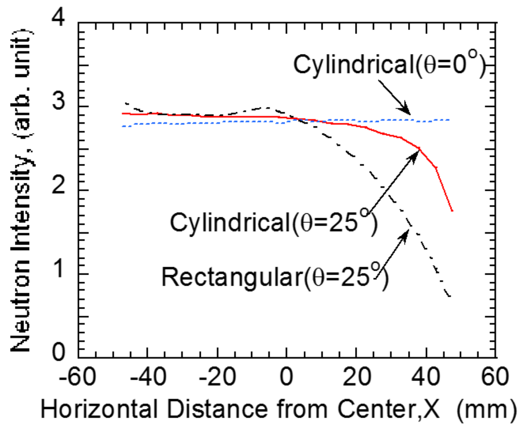

Fig. 6 Comparison of one-dimensional projections of the calculated vector flux of neutron intensities from cylindrical and rectangular-shaped moderators. The X-axis represents the distance from the axis of the moderator surface to the sample position of neutron instrument [16].

For the decoupled and poisoned moderators, a thermal neutron absorber, termed the "decoupler", plays an important role in forming a neutron pulse with a short decay time. At J-PARC, a silver-indium-cadmium (Ag-In-Cd) alloy [18] was used because boron-based materials such as sintered boron carbide (B_4C) cannot be used for a MW-class source because of the helium embrittlement caused by (n, α) reactions. As the Ag-In-Cd alloy is a combined material with numerous resonance-energy absorptions, it yielded an effective decoupling energy of 1 eV. For heat removal and corrosion protection, the Ag-In-Cd plate had to be bonded to the Al alloy (A5083) that is the structural material of the moderator and reflector. We adopted a hot isostatic pressing (HIP) method [19, 20] and succeeded in obtaining the required bonding. The thickness of the Ag-

In-Cd layer was determined to be 3 mm for it to survive longer than the estimated lifetime of the aluminum alloy for 6 MWy of irradiation time in the high-radiation environment of the present target-moderato-reflector system.

Figure 7 shows the partly cut-away 3D images of the decoupled and poisoned moderators. For the poisoned moderator, a 2-mm-thick Cd plate was installed inside the moderator vessel. To validate the neutronic performance of the Ag-In-Cd decoupler, the pulse shape in the rise and tail part of the Bragg peaks was observed at the neutron beamline BL10, "NeutrOn Beam-line for Observation and Research Use" (NOBORU), [21] at J-PARC. Figure 8 shows that the measured and calculated time structures of the neutron pulse at 1.86 meV are in good agreement [17].

For the pulse characteristics provided by the poisoned moderator, a resolution of $\Delta d/d = 0.035\%$ was obtained [17], where d is the lattice-spacing of reflection from the diffraction pattern from a silicon sample measured at the neutron beamline BL09, "super high-resolution powder diffractometer" (SuperHRPD) [22] over the long neutron flight path of 94.2 m. This resolution is outstanding; it is superior to the value of 0.04% obtained at the ISIS facility [23] in the UK.

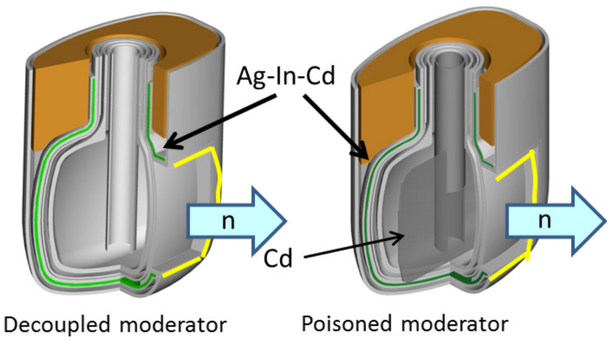

Fig. 7 3D views of decoupled (left) and poisoned (right) moderators. The Ag-In-Cd alloy decoupler location is indicated by the green line.

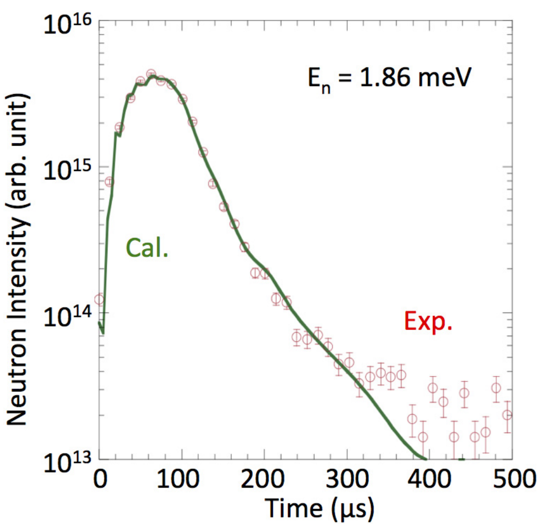

Fig. 8 Time structure of the neutron pulse at 1.86 meV measured at the neutron instrument BL10 [17]. The solid line shows the calculated result.

4. Efforts to Improve the Robustness of the Target Vessel

Figure 9 shows a view of the target vessel. The inner mercury vessel is covered with a water shroud, with an interstitial helium layer as a barrier against a leak from the mercury vessel. Mercury flows into the mercury vessel from the left rear toward the front of the target, sweeps across the front (the beam window), and then returns to the rear, following the shape of the vessel. The mercury flow is adjusted with flow vanes in the vessel, resulting in a mercury flow rate of 41 m^3/h, which can remove a heat load of 0.5 MW during a 1-MW operation. The thickness of the front part of the mercury vessel is 3 mm. The design pressures are 0.5 MPa each for the mercury, helium layer and water channel. Because of the stress and deformation of the vessel under such conditions, the water shroud was jointed to the mercury vessel with bolts, with a rib structure adopted as the interface between the inner water shroud and the mercury vessel.

4.1 Cavitation-damage-mitigation with gas microbubbles

At J-PARC, a gas-micro-bubble injection technique has been developed to mitigate the cavitation damage caused by the pressure waves generated in the mercury.

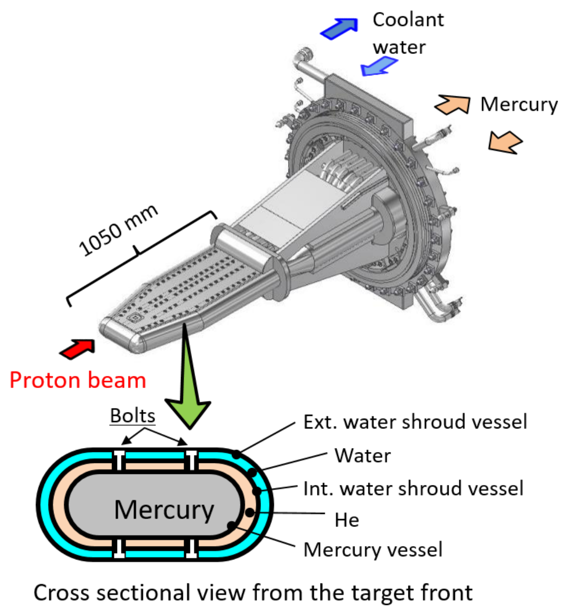

Fig. 9 Schematic illustration of the mercury target vessel, including a cross-sectional view.

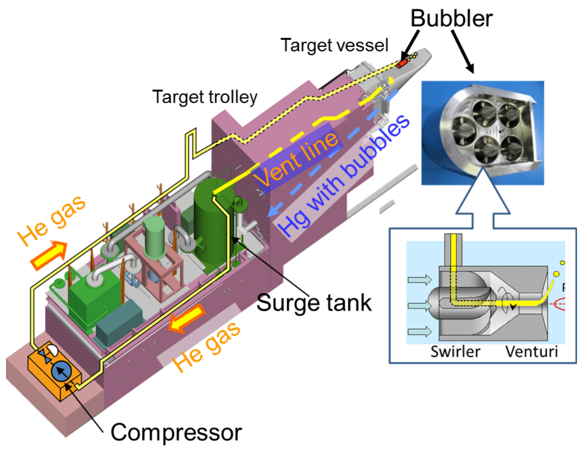

Fig. 10 Schematic of the mercury circulation system. Pictures of the swirl bubbler are also included.

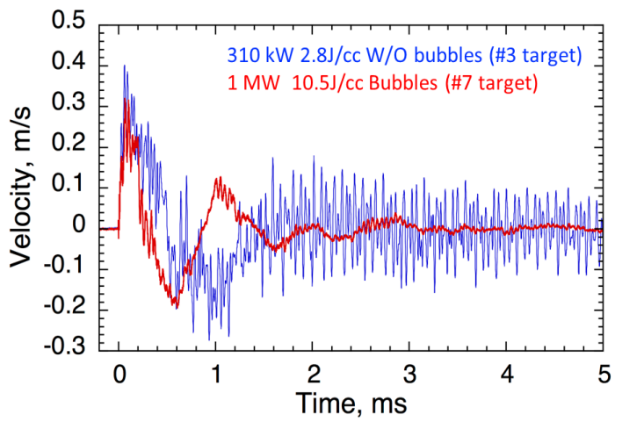

Fig. 11 Displacement velocities of the mercury target vessel measured with a Laser Doppler Vibrometer.

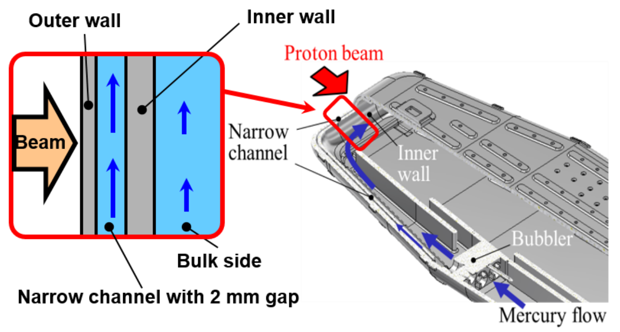

Fig. 12 Schematic of the mercury vessel with the narrow flow channel on the target front end.

The maximum pressure in the mercury reaches 40 MPa within 1 µs after the 1-MW proton beam is injected. This value is approximately 2.4 times higher than that generated in the mercury target of the SNS because of the difference in the repetition rates: 25 Hz at J-PARC *vs.* 60 Hz at SNS. Mitigation mechanisms provided by the micro-bubbles are as follows: 1) absorption of the thermal expansion of the mercury at the point of incidence of the proton beam and 2) attenuation of the pressure waves by volume oscillations of the bubbles and the thermal dissipation between the bubbles and the mercury.

Studies have demonstrated through off-beam [3] and on-beam [4, 5] experiments that the pressure wave could be effectively mitigated by supplying micro-bubbles with radii less than 100 µm so as to occupy a void fraction of 0.01% at the front end of the target vessel. To meet this requirement, a swirl-type-bubbler [6] was developed, into which gas is injected from the center of a static swirler, causing the gas column to broken down into microbubbles because of the shear force induced by vortex-breakdown at the outlet of the bubble generator. Multiple bubble generators with opposite swirl directions were alternately positioned to prevent bubble coalescence due to the bulk swirling flow. Figure 10 shows an illustration of the mercury circulation system. The helium gas enclosed in the surge tank is pressurized by a compressor and flows towards the bubbler in the target vessel.

Figure 11 shows the displacement velocity measured on the target vessel with a Laser Doppler Vibrometer [24] at the moment a pulsed proton beam is injected. The displacement velocity for the 1-MW case with the gas-micro-bubble injection (red line) is equivalent to the velocity obtained for the 310-kW case without gas-micro-bubble injection (blue line), indicating that the pressure wave generated in the mercury during 1-MW operation can be reduced by a factor of there by gas-micro-bubble injection.

4.2 Cavitation-damage-mitigation with narrow channel flow

In 2014, we started using a target vessel with a double-walled beam window to obtain further tolerance against the pressure waves [7]. Figure 12 shows an image of the mercury vessel with the double-walled target front end. Part of the mercury flow goes without passing through the bubbler into a narrow 2-mm-wide channel formed by the double wall, and the flow velocity is approximately 4 m/s [8]. The rest of the flow, called the “bulk flow”, passes through the bubbler and advances to the inner wall with the entrained micro-bubbles. This enhances the cooling of the inner wall, enabling an increase in the wall thickness from 3 to 5 mm and increasing the safety margin against the cavitation damage.

Off-beam tests using a small mercury loop [25] have showen promising results, indicating that cavitation damage is considerably mitigated by the fast flow in the narrow channel. This was also demonstrated in on-beam tests conducted at the WNR facility at the Los Alamos National Laboratory, in collaboration with the target-development group from ORNL [4]. The mitigation is due to the flowing mechanisms: 1) the wall of the narrow channel wall

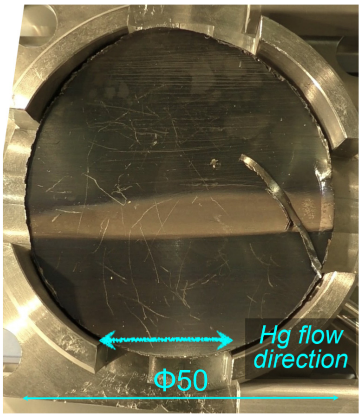

Fig. 13(a) Photo of a specimen cut from a target vessel with a double-walled narrow channel.

impedes the growth of cavitation bubbles, as they cannot expand fully and 2) the faster mercury flow deforms the cavitation bubbles, leading to a defocusing of the force exerted to the target wall when the bubble collapses, in contrast to the case for normal spherical bubbles. At the SNS, a mercury target with a double-walled front end has been operating at 1 MW or more during the scheduled operational periods [11]. For the SNS target, a mercury flow of ca. 3 m/s sweeps the surface of the beam-window wall and obvious pitting damage has not been observed, although the inner-wall surface facing to the low-velocity bulk mercury flow was significantly damaged.

To study the effect of the narrow channel on the cavitation-damage mitigation during the target operation, we cut out a specimen from a target vessel which had been irradiated for 670 MWh at an average power of 402 kW. This was the first observation of the outmost 3-mm- thick wall of a mercury vessel with a narrow flow channel. As shown in Fig. 13 (a), visual inspection revealed that the surface roughness of one area changed along the direction of the mercury flow [26]. Inspection using a laser scanning microscope (LSM) (Keyence, VK-9510) revealed that cavitation damage likely occurred on that area. Moreover, a silicone-rubber surface replica (Struers, Repliset-F1) was used to measure the surface roughness of the specimen for a detailed evaluation of the cavitation damage. Hence, we concluded that the band-like damage was probably caused by the accumulation of pits caused by the cavitation. Around the center of the band-like damage, relatively deep pits were distributed among the accumulated pits, as shown in Fig. 13 (b). The maximum depth of a pit was approximately 25 µm [27]. This depth is slightly deeper than the predicted damage depth of approximately 10 - 15 µm, based on a prediction method proposed in a previous study [28].

The duration of the irradiation and the power for this specimen is still very low compared with the planned lifetime of 5000 MWh. Since the lifetime of the outmost wall

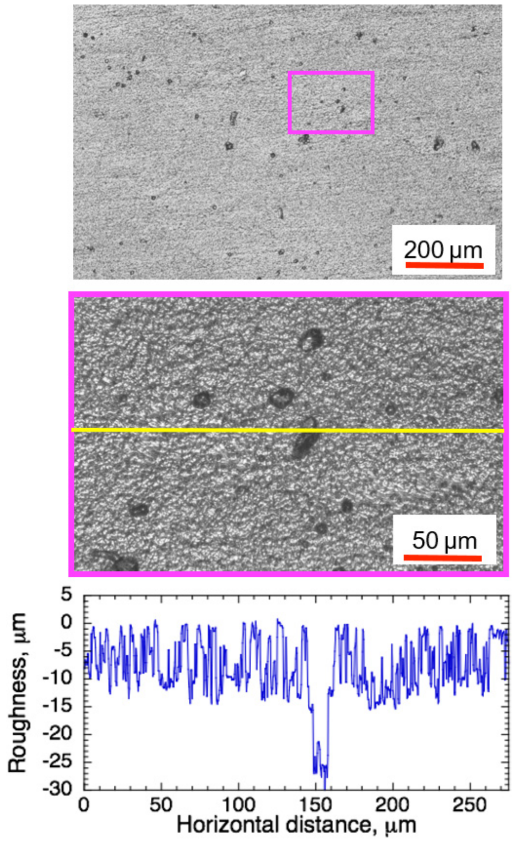

Fig. 13(b) Confocal images and depth profiles at the center of band-like damage on the specimen shown in Fig. 13 (a) [27].

is critical for the operation of the target system, further study of the mechanism of this cavitation damage is important.

4.3 Redesign of the mercury target vessel

In 2015, the water shroud around the mercury vessel failed during operation at 500 kW. The failure location was identified by visual inspection by pressurizing the cooling channel of the water shroud. A line-shaped flaw was found on the bottom surface, and water drops leaked from a point on the flaw. Figure 14 illustrates the location of the failure in the water-shroud structure. The failure point was located beside one of the bolts jointing the water shroud and the mercury vessel. As shown in Fig. 14, the diffusion-bonding interface contributes in strengthening the coolant boundary against the stress load.

We were unable to cut out samples from the actual target because it was highly radioactive and contained a large amount of radioactive gases, such as ^{3}H. Consequently, the cause of failure was investigated using analyses and mockup tests, which took into account the fabrication process [29]. Because the failure occurred after the target had been in operation for approximately four months, we concluded that fatigue failure had occurred due to the repet-

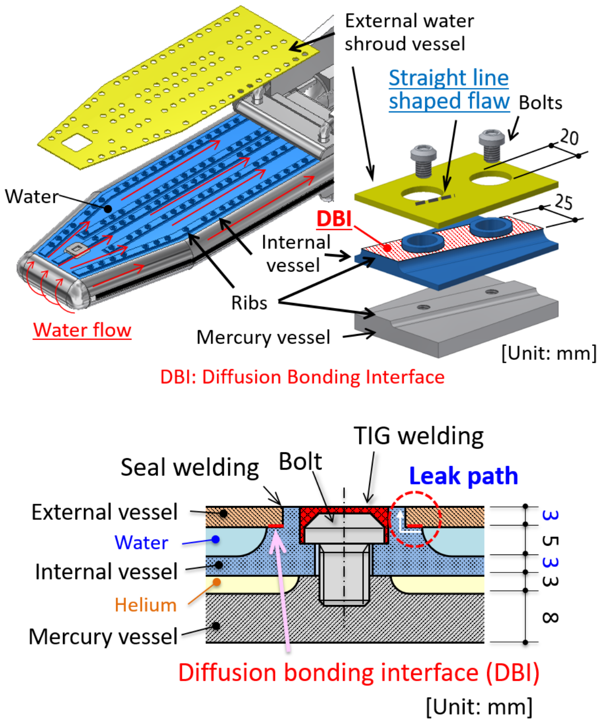

Fig. 14 Schematic illustration of the water-shroud structure of the target vessel. Details of part of a rib structure are illustrated at the upper right, and a cross-sectional view of a bolt joint between the water shroud and the mercury vessel is shown in the lower panel.

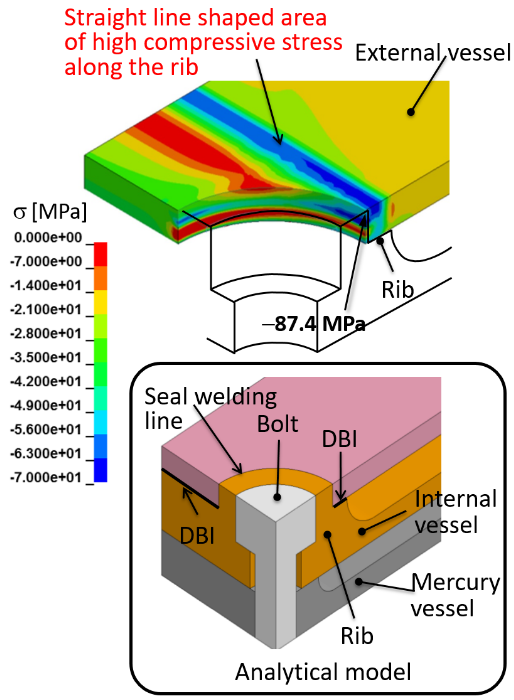

Fig. 15 Analytical result for the compressive thermal stress generated by the temperature swing in the water shroud at a 1.5-mm-deep seal weld between proton beam injections and trips. The lower panel illustrates a model covering one-quarter of the structure around the bolt, as shown in Fig. 14.

itive temperature swings induced when the proton beam trips. The following fabrication processes may have caused the leak path: 1) The sealing weld only filled to the interface line without making a groove, which means that it did not guarantee that the complete weld conformed to 3-mm plate thickness. 2) The diffusion-bonding interface has a narrow width, less than 2.5-mm wide, around the periphery of the bolt on the 20-mm-wide rib, although it has sufficient area in the longitudinal direction. It received a large heat input when the bolt head was welded using TIG welding after the seal-performance tests for the diffusion-bonding process had been completed.

Analytical studies were performed with the conventional code, LS-DYNA, assuming that the materials are elastic, using a model that covered one-quarter of the structure around the bolt, as shown in Fig. 15. For the simulation, the initial temperature of the bolt head was set at 1400°C, which is the melting point of stainless steel, and a tensile stress significantly larger than the yield strength of stainless steel was generated at the diffusion bonding interface. Furthermore, the simulation showed that large tensile stress was generated along the seal-welding line for an insufficient weld depth of 1.5 mm, when the temperature dropped to the room temperature after the proton beam was tripped during operation. The simulation also demonstrated that a compressive thermal stress of 87.4 MPa was loaded at the lower edge of the weld depth, and it was distributed in a straight-line shape along the rib as shown in Fig. 15. These results suggest that the possible mechanism of failure was the breaking of diffusion bonding during the TIG welding of the bolt head and that initial defects at the diffusion bonding and at the seal weld grew to form the leak path as thermal stress is repetitively loaded when proton beam is tripped during operation. In fact, such defects were observed in the diffusion-bonding interface of a test piece prepared using the same fabrication process as for the actual water shroud.

Based on these findings, we have redesigned the target vessel structure to ensure its robustness. Figure 16 shows a schematic of the redesigned target vessel. The important objective is to reduce the number of weld lines to a minimum. Improved fabrication and inspection are also required to avoid leaving defects. In the redesigned target vessel, the forward part of the mercury vessel and the water shroud have been changed to be monolithic structure to eliminate welds and bolts from high-stress regions, although the rib structure between the mercury vessel and the water shroud remains. These changes have decreased the total length of the welding lines down to 55% compared with that in original. For the rear part of the target vessel, the upper and lower plates of the water shroud have also been changed to monolithic structures. In addition,

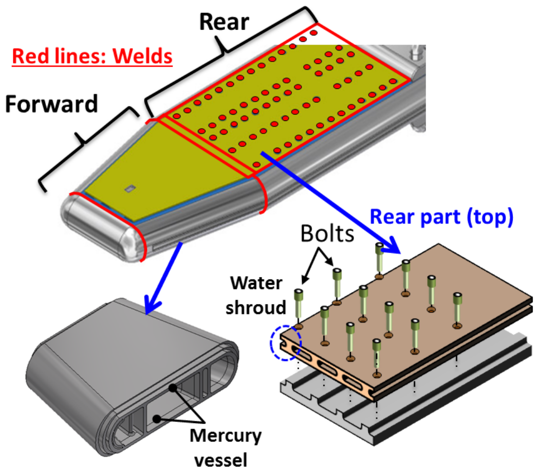

Fig. 16 Schematic of the redesigned target vessel structure. The forward part of structure and the rear part of the water shroud have both been changed to monolithic structures.

inspection processes were also improved to include numerous radiation and ultrasonic tests. Further design study will be required to change the target-vessel structure so that the water shroud is completely separated from the mercury vessel, termed "constraint-free structure", because it is a simple structure with a minimum number of welds.

5. Summary

At the pulsed spallation neutron source at J-PARC, the neutron-pulse characteristics delivered from the moderators have been measured during low-power operation, and the measured data are in good agreement with the calculated neutron intensities. This indicates that a peak intensity as high as 4.5×10^{12} n/cm^2/s/sr can be provided from a coupled moderator containing 100% para-hydrogen at a rated proton-beam power of 1 MW. In addition, neutron pulses with the superior resolution of $\Delta d/d = 0.035\%$ can be provided from the poisoned moderator.

To achieve 1-MW operation, we have to overcome issues related to the mercury-target operation, such as cavitation-damage mitigation. At present, redesign of the target vessel is an urgent issue to recover operational beam powers higher than 500 kW because we encountered a failure of the water shroud of the target vessel in 2015. The new target vessel, which eliminates welds and bolt joint from high-stress regions in the front half of the target vessel is in use from October in 2017. Cavitation-damage mitigation using a gas-micro-bubble technique and fast mercury flow will be studied during target operation, and further design upgrades will improve the robustness of the target.

Acknowledgments

The author would like to thank the staff of neutron source section of the J-PARC center of JAEA for their contributions to the target-moderator-reflector system operations, maintenance, and design upgrades of the components. He is also thankful to Enago (www.enago.jp) for the English language review.

[1] H. Takada *et al.*, Quantum Beam Science **1**, 8 (2017).
[2] F. Maekawa *et al.*, Nucl. Instrm. Methods Phys. Res. A **620**, 159 (2010).
[3] M. Futakawa *et al.*, J. Nucl. Sci. Technol. **45**, 1041 (2008).
[4] B. Riemer *et al.*, J. Nucl. Mater. **377**, 162 (2008).
[5] B. Riemer *et al.*, J. Nucl. Mater. **450**, 192 (2014).
[6] H. Kogawa *et al.*, J. Nucl. Sci. Technol. **56**, 1461 (2015).
[7] M. Futakawa, JPS Conf. Proc. **8**, 0010002 (2015).
[8] H. Kogawa *et al.*, J. Nucl. Sci. Technol. **54**, 733 (2017).
[9] K. Haga *et al.*, JPJ Conf. Proc. **8**, 051008 (2015).
[10] J.R. Haines *et al.*, Nucl. Instrm. Methods Phys. Res. A **764**, 94 (2014).
[11] B.W. Riemer *et al.*, Proceedings of the 11th International Topical Meeting on Nuclear Applications of Accelerators (AccApp 2013), Brugge, Belgium, August 5-8, 2013, pp.359-365 (2014).
[12] J-PARC Center, "J-PARC ANNUAL REPORT 2015 Vol.2: Materials and Life Science Experimental Facility", J-PARC 17-01, pp.54-55 (2017).
[13] M. Tamura and F. Maekawa, JAERI-Tech 2003-010 (2003) (in Japanese).
[14] R.E. MacFarlane *et al.*, LA-12639-MS (1994).
[15] T. Kai *et al.*, Nucl. Instrum. Methods Phys. Res. A **523**, 398 (2004).
[16] T. Kai *et al.*, Nucl. Instrum. Methods Phys. Res. A **550**, 329 (2005).
[17] F. Maekawa *et al.*, Nucl. Instrum. Methods Phys. Res. A **620**, 159 (2010).
[18] M. Teshigawara *et al.*, J. Nucl. Mater. **343**, 154 (2005).
[19] K. Kikuchi *et al.*, Mater. Sci. Forum **652**, 92 (2010).
[20] M. Harada, J. Nucl. Mater. **398**, 93 (2010).
[21] F. Maekawa *et al.*, Nucl. Instrum. Methods Phys. Res. A **600**, 335 (2009).
[22] T. Kamiyama and K. Oikawa, Proc. 16th Int. Collaboration Mtg. Advanced Neutron Sources, Dusseldorf-Neuss, Germany, May 12-15, ISSN 1433-559X, 309 (2003).
[23] W.I.F. David and M.W. Johnson, Proc. 8th Int. Collaboration Mtg. Advanced Neutron Sources, Rutherford Appleton Laboratory, UK, 427 (1985).
[24] M. Teshigawara *et al.*, J. Nucl. Mater. **398**, 238 (2010).
[25] T. Naoe and M. Futakawa, Trans. JSME **80**, fe0025–1 (2014) (in Japanese).
[26] H. Takada *et al.*, Proc. AccApp'15, Washington DC, USA, November 10-13, 2015, p.297 (2016).
[27] T. Naoe *et al.*, 13th Int. Workshop on Spallation Materials Technologies, Chattanooga, Tennessee, USA, Oct. 30 - Nov. 4, 2016 (in press in J. Nucl. Mater.). https://doi.org/10.1016/j.jnucmat.2017.12.019
[28] T. Naoe *et al.*, J. Nucl. Mater. **468**, 313 (2016).
[29] K. Haga *et al.*, J. Nucl. Sci. Technol. **55**, 160 (2018).